Segmentation of Zebrafish Larva Inhomogeneous 3D Images Using the Level-Set Method

Zhan Xiong; Advanced Computer science Institute of Leiden University; Leiden, Netherlands;
Fons J. Verbeek; Imaging & BioInformatics, Leiden Institute of Advanced Computer Science, University; Leiden, Netherlands
Email: {***z.xiong, f.j.verbeek***}***@liacs.leidenuniv.nl***

Abstract

Image local information is crucial for accurate segmentation of images with inhomogeneities in the intensity. In many popular methods, however, local regional information is normally underestimated and not included in the segmentation framework. In this paper, a segmentation is formalised as Bayesian Inference procedure. By considering the spatial variation of the intensity distribution, a likelihood that contains a joint distribution of intensity and spatial location is obtained. After incorporating this likelihood in a Bayesian maximum a posteriori estimation, we transformed the stochastic model into a segmentation method which utilises local information to segment images with inhomogeneities so as to guarantee a global optimum for the two-region case(foreground/background). Taking the computational complexity of our model into account, we take advantage of a GPU parallel algorithm to accelerate computation without losing segmentation accuracy. We demonstrate that taking into account local image information, our method results in significant improvements for image segmentation.

Introduction

In the life sciences, images are an important source of information in the study of the processes of life. Here we are particularly interested in microscopy images and images of specimens made with microscopes are not always ideal for further numerical analysis. Therefore image restoration and enhancement techniques are required to be able to extract the right information from the images. We are specifically interested in accurately extracting 3D objects from volume data produced by confocal laser scanning microscopy (CLSM). The objects in CLSM are fluorescently labelled which discriminate an object from the background. However, the homogeneity in the fluorescent staining is not always stable and/or constant. This gives rise to problems in the extraction of the object, i.e. the segmentation is a difficulty to overcome. We, therefore, want to address this problem by finding an effective optimization model for the segmentation of 3D objects.

There are a number of algorithms, including watershed, thresholding, clustering, and so on, that can be applied to segment inhomogeneous 3D objects. The common starting point for these algorithms to work properly is that voxels belonging to an object should have a homogeneous intensity [9, 11, 12, 13]. Thus, these algorithms are not capable of extracting objects from images that exhibit an inhomogeneous distribution, e.g. Fig.1. In addition, some intrinsic limitations in fluorescence imaging, such as photobleaching, chromatic and spherical aberration, blurring and non-continuous and low signal-noise ratio will further invalidate those existing methods.

In the life sciences, the availability of well-defined procedures for extraction of information from images, has been acknowledged as an important topic in bio-imaging [5, 6, 7]. In our research we investigate zebrafish larvae that are stained through a reporter marker, i.e. GFP [8]. Although the fluorescent label provides an indication of the zebrafish larvae in the image, the distribution of the fluorescent label is not homogeneous and also not continuous. In the interpretation of these images, one step is to interpolate missing voxels over the inhomogeneity and discontinuities, the feature of human vision should be reflected in the method to extract the objects, i.e. the zebrafish, from the image. Moreover, the object extraction should be completed automated and in a reasonable time. So, our efforts are directed at developing an accurate and time efficient method for object extraction from fluorescent image, in particular, 3D images of zebrafish larvae.

In the research presented here, we choose a level set method as numerical implementation framework for tracking boundaries and shapes as it is able to represent surfaces with complex topologies and evolve their topology in a natural way. Existing level set methods for image segmentation can be categorized into two major classes: region-based models [9, 10, 12], and edge-based models [11, 21, 26]. Region-based models aim to identify each region of interest by using a certain region descriptor to guide the motion of the active contour. It is, however, very difficult to describe a region with intensity inhomogeneities. A typical region-based example are the piecewise constant (PC) models proposed in [9]. Edge-based models use edge information for image segmentation. These models do not assume homogeneity of image intensities, and thus might be applied to images with intensity inhomogeneities. However, these type of methods are, in general, quite sensitive to the start conditions and often suffer from serious "leakage" problems where with weak object boundaries are present in the images[26].

Key to overcome difficulties with inhomogeneity in the image is the use of local regional image information. Using a generally accepted model of images with intensity inhomogeneities, we present a probabilistic framework, in which local information that is understood as the intensities in a neighbourhood of which each point is interpreted as a conditional probability and embedded as a part of a posteriori

probability in Bayesian inference model[28]. Furthermore, the maximal Bayesian a posteriori probability transformed into a novel region-based level-set function where local information is integrated over the neighbourhood centre to define an energy functional. Minimization of this energy is achieved by an evolution process of level set evolution. Hence, the relevant local information is utilized in a mathematical way. In order to reduce computation complexity, this algorithm is specifically designed to segment a 3D object from raw 3D images in a parallel manner.

This paper is organized as follows. In Section II we present the inferring stochastic framework and show local image information is integrates. It contains the mathematical foundation of the optimization of the energy function. In Section III we focus in detail on the two-region energy function and the formulation of the level-set method, the main algorithm in our research. In Section IV, the level set formulation and the numerical implementation of iteratively partial derivative, GPU parallelisation as well as experimental results are presented. Finally, in section V we present our conclusion and discussion.

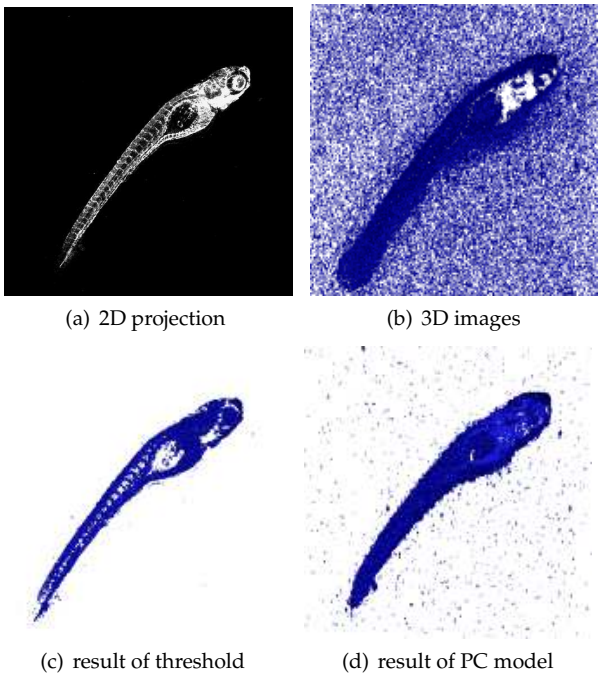

(a) 2D projection (b) 3D images

(c) result of threshold (d) result of PC model

Figure 1: Error of thresholding and PC model for images with intensity inhomogeneity. (a)-(b): Original data in 2D project and 3D with noise; (c)-(d): the result of Thresholding and PC model.

A Statistical Framework for Segmentation

In this section, we will derive a maximum likelihood estimation in the context of Bayesian inference formulation and transform this stochastic estimation into a region-based energy function. In this stochastic model, intensity likelihoods of partitioned regions are not constant, but vary along its locations. One of the challenges addressed in this paper is the embedding of local information derived from an inhomogeneous data set into a formulation of Bayesian inference .

Approach to Segmentation as Bayesian Inference

Let $I \rightarrow \mathbb{R}^d (d = 1 \; or \; 3)$ denote the input data defined on the domain $\Omega \subset \mathbb{R}^s (s \geq 2)$. The task of segmenting the image space into a set of n pairwise disjoint regions Ω_i:

$$\Omega = \bigcup_{i=1}^{n} \Omega_i, \; \Omega_i \cap \Omega_j = \emptyset, \forall i \neq j \tag{1}$$

can be solved by computing a labelling $\theta : \Omega \rightarrow \{1, \cdots, n\}$, indicating which of the n regions each vector $\mathbf{x}$ belongs to: $\Omega_i = \{\mathbf{x} | \theta(\mathbf{x}) = i\}$, and an approximation u, depicting what a intensity-space joint distribution of the n regions is: $u_i(\mathbf{x}) = \{u(\mathbf{x}) | \theta(\mathbf{x}) = i\}$. In the framework of Bayesian inference, one can compute such a segmentation by maximising the conditional probability:

$$\arg\max_{\theta} \mathcal{P}(\theta, u|I) = \arg\max_{\theta} \frac{\mathcal{P}(u|I,\theta) \cdot \mathcal{P}(I|\theta) \cdot \mathcal{P}(\theta)}{\mathcal{P}(I)} \tag{2}$$

where $\mathcal{P}(I)$ is a constant, which is irrelevant to the maximisation of conditional probability. A straightforward interpretation that arises from the above formulation is that if one intends to obtain a most likely configuration of label θ over the whole image domain Ω, alongside the corresponding most reasonable approximation u under given input data I, we could substitute a Bayesian a posteriori probability computation. Here, for a fixed label configuration and an input image domain, $\mathcal{P}(u|I,\theta)$ indicates the extent of the probability an approximation showing up; $\mathcal{P}(I|\theta)$ represents, in a specified distribution and at a given label configuration θ, the probability of I is; $\mathcal{P}(\theta)$ represents prior knowledge that a label configuration θ should have, such as the smoothness property along boundaries between different regions.

Assuming that the intensities of all $\mathbf{x}$ in u is not independent, but, in contrast to previous segmentation approaches[11, 24, 25, 26], is dependent on space, we obtain

$$\mathcal{P}(u|I,\theta) = \mathcal{P}(u(\mathbf{x}), \mathbf{x}|I,\theta) \tag{3}$$

where $u(\mathbf{x})$ and vector $\mathbf{x}$ individually indicate the approximated intensity and vector location in Ω. If we, furthermore, take the hypothesis that the intensity probability at location $\mathbf{x}$ is only influenced by its neighbours within Ω_i rather than vectors affiliated to other regions $\Omega_j (j \neq i)$, the probability in Eq.(3) can be extended as

$$\mathcal{P}(u|I,\theta) = \prod_{i=1}^{n} \mathcal{P}(u(\mathbf{x}), \mathbf{x}|I,\theta_i) \tag{4}$$

Note that Eq. (4) shows $u(\mathbf{x})$ is variant in region Ω_i instead of being constant as it normally is[9]. It has commonly been neglected, but we will show here that taking into account this spatial variation of intensity distributions based on a weighted spatial kernel density leads to drastic improvements of the resulting segmentation process.

Supposing the probability of $I(\mathbf{x})$ is only relevant to $\theta(\mathbf{x})$, $I(\mathbf{x})$ and $\theta(\mathbf{x})$ should obey a bivariate distribution. Let $Q_{\rho,\sigma}(\cdot)$ denote the kernel density function with ρ and σ as parameters, we get

$$\mathcal{P}(I|\theta) = \prod_{i=1}^{n} \mathcal{P}(I|\theta_i) \propto \prod_{i=1}^{n} \exp\Big(Q_{\rho,\sigma}(u_i(\mathbf{x}), I(\mathbf{x}))\Big) \tag{5}$$

where $u_i(\mathbf{x})$ is the estimated value in region Ω_i. Eq. (5) can be interpreted as the more likely $\mathbf{x}$ belongs to Ω_i, the smaller intensity difference between $I(\mathbf{x})$ and $u(\mathbf{x})$ at a given location $\mathbf{x}$ in Ω_i is. In practice, it is used as the data fidelity term to assure the approximation u remains highly analogous to I.

Prior knowledge is considered as a powerful regularisation mechanism to limit our solution into a comparatively narrow but yet reasonable scope. We could specify the prior $\mathcal{P}(\theta)$ to favour segmentation regions of shorter boundaries:

$$\mathcal{P}(\theta) \propto \exp\left(\sum_{i=1}^{n} \mathcal{L}(\Omega_i)\right) \tag{6}$$

where $\mathcal{L}(\Omega_i)$ denotes the length of the boundaries of each region $\Omega_i = \{\mathbf{x} \in \Omega | \theta(\mathbf{x}) = i\}$.

Inferring Space-Variant Intensity Distributions

The expression in Eq. (4) denotes the joint probability for observing a intensity value I at the given $\mathbf{x}$ being part of region Ω_i. It can be estimated as

$$\mathcal{P}(u(\mathbf{x}), \mathbf{x}|I, \theta_i) \propto \exp\left(\int_{\Omega_i \setminus \mathbf{x}} G_{\rho,\sigma}(u_i(\mathbf{x}), I(\mathbf{y}))\mathrm{d}\mathbf{y}\right) \tag{7}$$

where, $G_{\rho,\sigma}(\cdot)$ denotes a kernel function centred at given $\mathbf{x}$. With a hypothesis that, as a space-variant kernel function, $G_{\rho,\sigma}(\cdot)$ will proportionally vary to the intensities and locations. This kernel states that at a given centre $\mathbf{x}$ in region Ω_i, $u_i(\mathbf{x})$ is a weighted sum of all its neighbour $I(\mathbf{y})$ in region Ω_i, whose weight coefficients are dominated by the distance of $\mathbf{y}$ against centre $\mathbf{x}$. Hence, we could construct a Gaussian intensity distribution having a spatial-variant property. Note that in our model, $u_i(x)$ is determined by its neighbours in the same region without itself, which could simplify the stochastic model.

The negative logarithm of the estimated probability distributions can be used as a powerful data-term for segmentation. For each centre $\mathbf{x}$ we obtain the data-term by adding all regional terms over its region Ω_i

$$\mathcal{E}(\mathbf{x}) = \sum_{i=1}^{n} \mathcal{E}_i(\mathbf{x}) = \sum_{i=1}^{n} -\log\left(\mathcal{P}(u|I, \theta_i) \cdot \mathcal{P}(I|\theta_i)\right) \tag{8}$$

The proposed formulation can be seen as a generalisation of the traditional purely intensity-based approaches. By steering ρ and σ, the parameters in kernel density functions $Q_{\rho,\sigma}(\cdot)$ and $G_{\rho,\sigma}(\cdot)$, we can scale the influence of intensity similarity and location distance on the segmentation result.

Formulation of the Variation Method

Having determined the probability distributions from every $\mathbf{x}$ for all regions Ω_i, $i = 1, \cdots, n$, we are now ready to solve the maximization of optimization/labelling problem Eq. (2) equivalently by minimizing its negative logarithm (cf. Eq. 8). According to Eq.(6) and Eq.(8), the maximum a posteriori (MAP) estimation is equivalent to solve the minimization of the energy function

$$\mathcal{E}(\Omega_1, \cdots, \Omega_n) = \nu \sum_{i=1}^{n} \mathcal{L}(\Omega_i) + \lambda \int_{\Omega} \mathcal{E}(\mathbf{x})\mathrm{d}\mathbf{x} \tag{9}$$

in which λ and ν are positive weighting parameters that regulate the influence of the data-term and regulariser.

Note that this maximisation of a posteriori probability formulation works as a generalised energy function to solve segmentation problem. Through adjusting different $Q_{\rho,\sigma}$ (deferred intensity distribution) in Eq.(5) and $G_{\rho,\sigma}$ (satisfied space-variant intensity distribution) in Eq.(7), we can embed different image information into our Bayesian inference formula and generate a corresponding optimisation object function.

Local Regional Energy Function and Level-Set Formulation

In this section, we will develop a concrete pair of $Q_{\rho,\sigma}$ and $G_{\rho,\sigma}$ to fit an inhomogeneity labelling problem. In our research, we only considered a two-region label problem. In this case, global optimisers can always be found[14]. Consequently, our aim is to seek an optimal approximation from input data under the condition of an inferred energy function.

Inferring Objective Energy Function

Our goal is to find an optimal approximation from inhomogeneous input data, therefor local information should be extracted from each region and embedded into our energy function to enhance discrimination ability of blurry foreground voxels from background noise, and subsequently ensuring the approximation u could analogous to I. To this end, we could construct a space-variant kernel function $G_{\rho,\sigma}(\cdot)$ and intensity distance kernel function $Q_{\rho,\sigma}(\cdot)$ as follows:

$$G_{\rho,\sigma}(u_i(\mathbf{x}), I(\mathbf{y})) = K_\rho(\mathbf{x}-\mathbf{y})\frac{|I(\mathbf{y}) - u_i(\mathbf{x})|^2}{2\sigma^2} \tag{10}$$

and

$$Q_{\rho,\sigma}(u_i(\mathbf{x}), I(\mathbf{x})) = K_\rho(\mathbf{x}-\mathbf{x})\frac{|I(\mathbf{x}) - u_i(\mathbf{x})|^2}{2\sigma^2} \tag{11}$$

where $u_i(\mathbf{x})$ is the approximated intensity at the point $\mathbf{x}$ in region Ω_i; $K_\rho(|\mathbf{x}|)$ is a kernel function with a spatial property that decreases and approaches zero as $|\mathbf{x}|$ increases. Here, we choose the kernel function $K_\rho(\cdot)$ as a Gaussian kernel with a scale parameter $\rho > 0$:

$$K_\rho(\mathbf{x}) = \frac{1}{(2\pi)^{n/2}\rho^n} e^{-|\mathbf{x}|^2/2\rho^2} \tag{12}$$

Note that with this definition, $Q_{\rho,\sigma}(u_i(x), I(x))$ equals $G_{\rho,\sigma}(u_i(x), I(x))$, which drastically simplifies our model through combination local information with a data fidelity term. According Eq.(10) and Eq.(11), we accomplished the data-term $\mathcal{E}$ in each region Ω_i from Eq.(8) as follows:

$$\begin{aligned}\mathcal{E}_i(\mathbf{x}) &= \int_{\Omega_i \setminus \mathbf{x}} G_{\rho,\sigma}(u_i(\mathbf{x}), I(\mathbf{y}))\mathrm{d}\mathbf{y} + G_{\rho,\sigma}(u_i(\mathbf{x}), I(\mathbf{x})) \\ &= \int_{\Omega_i} G_{\rho,\sigma}(u_i(\mathbf{x}), I(\mathbf{y}))\mathrm{d}\mathbf{y}\end{aligned} \tag{13}$$

It should be emphasised that $u_i(\mathbf{x})$ is the function of a centre $\mathbf{x}$ and will vary with the centre $\mathbf{x}$ due to the fact that the kernel function $K_\rho(\cdot)$ takes larger values at location $\mathbf{y}$ near the centre $\mathbf{x}$, and it decreases to 0 as $\mathbf{y}$ goes away. Therefore, an influence on $u_i(x)$ increases in dominance when $\mathbf{y}$ is approaching the vicinity of centre $\mathbf{x}$, whereas it gradually fades out if $\mathbf{y}$ retreats from the centre.

Let C be a contour in the domain Ω, in 3D segmentation, C is actually the boundary surface between different regions, but in the context of level-set framework, for coherence we continue to use the contour concept. Obviously, for each centre $\mathbf{x}$, the regional energy $\mathcal{E}_i(\mathbf{x})$ can be minimised when C is exactly on the object boundary and the approximated values u_i are optimally chosen. In order to find the entire object boundary, we must minimise $\mathcal{E}_i(\mathbf{x})$ over all regions Ω_i. This can be achieved by minimising the total integral of $\mathcal{E}_i(\mathbf{x})$ over all the centres $\mathbf{x}$ in the domain Ω. So, we define the $\mathcal{E}(x)$ in Eq.(9) as follows:

$$\begin{aligned}\mathcal{E}(C, \mathbf{x}) = &\int_{in(C)} (2\sigma^2)^{-1} K_\rho(\mathbf{x}-\mathbf{y}) |I(\mathbf{y}) - u_1(\mathbf{x})|^2 \mathrm{d}\mathbf{y} \\ &+ \int_{out(C)} (2\sigma^2)^{-1} K_\rho(\mathbf{x}-\mathbf{y}) |I(\mathbf{y}) - u_2(\mathbf{x})|^2 \mathrm{d}\mathbf{y}\end{aligned} \tag{14}$$

This energy can be converted to an equivalent level-set formulation, from which an implicit active contour will be created to automatically handle topological changes.

Formulation of the Variational level-set model

In level-set methods[23], a contour $C \in \Omega$ is represented by the zero level-set of a Lipschitz function $\Phi : \Omega \to \mathbb{R}$. Hence, the original task, at present, has transformed into a label problem over an implicit function Φ. A Heaviside function is introduced as the global label configuration. Within the level-set representation, the energy functional $\mathcal{E}(C, \mathbf{x})$ in Eq.(14) can be rewritten as:

$$\begin{aligned}\mathcal{E}(\Phi, \mathbf{x}) = &\iint_{\Omega} K_\rho(\mathbf{x}-\mathbf{y}) \frac{\left|I(\mathbf{y}) - u_1(\mathbf{x})\right|^2}{2\sigma^2} H_1(\mathbf{y})\, \mathrm{d}\mathbf{y}\, \mathrm{d}\mathbf{x} \\ &+ \iint_{\Omega} K_\rho(\mathbf{x}-\mathbf{y}) \frac{\left|I(\mathbf{y}) - u_2(\mathbf{x})\right|^2}{2\sigma^2} H_2(\mathbf{y})\, \mathrm{d}\mathbf{y}\, \mathrm{d}\mathbf{x}\end{aligned} \tag{15}$$

where $H_1(\mathbf{x})$ and $H_2(\mathbf{x})$ are the composition of Heaviside function in a form of $H_i(\Omega(\mathbf{x}))$, and $H_1(\mathbf{x}) + H_2(\mathbf{x}) = 1$.

In order to avoid the level-set re-initialization problem[15] and ensure a stable evolution of the level-set function Φ, an extra distance regularization term proposed by Li[16] to penalise the deviation of Φ from a signed distance function is added in our variational level-set formulation. The distance regularization function is characterized by the following integral:

$$\mathcal{P}(\Phi) = \int_{\Omega} p(|\nabla\Phi|)\mathrm{d}\mathbf{x} \tag{16}$$

To regularise the contour in level-set energy functional, we also need the length of the zero-level curve (surface) of Φ, which is given by:

$$\mathcal{L}(\Phi) = \int_{\Omega} \delta(\Phi)|\nabla\Phi|\mathrm{d}\mathbf{x} \tag{17}$$

where smooth Dirac function $\delta(\Phi)$ is the deviation of Heaviside function $H(\Phi)$.

Now, we define the entire energy functional of all centres $\mathbf{x}$ over whole domain Ω

$$\mathcal{F}(\Phi, u_1, u_2) = \lambda\mathcal{E}(\Phi, u_1, u_2) + \mu\mathcal{P}(\Phi) + \nu\mathcal{L}(\Phi) \tag{18}$$

where λ, μ and ν are non-negative constants. By solving above optimization problem, a reasonable approximation which is able to tolerate inhomogeneity within each region will obtained, and consequently a relatively short yet smooth contour that partitioned foreground from background will be located at the boundary of the object.

Gradient Descent Flow

We use the standard gradient descent method, a.k.a steepest descent method, [17, 18] to minimize the energy functional Eq.(18). The detailed derivation of the gradient flow is given as follows:

- For a fixed level-set function Φ, we minimize the functional Eq.(18) with respect to the functions $u_1(\mathbf{x})$ and $u_2(\mathbf{x})$. By calculus of variations, it can be shown that the functions $u_1(\mathbf{x})$ and $u_2(\mathbf{x})$ that minimize $\mathcal{F}(\Phi, u_1, u_2)$ for a fixed function Φ are given by:

$$u_1(\mathbf{x}) = \frac{K_\sigma(\mathbf{x}) * [H_1(\mathbf{x})I(\mathbf{x})]}{K_\sigma(\mathbf{x}) * H_1(\mathbf{x})} \tag{19}$$

and

$$u_2(\mathbf{x}) = \frac{K_\sigma(\mathbf{x}) * [H_2(\mathbf{x})I(\mathbf{x})]}{K_\sigma(\mathbf{x}) * H_2(\mathbf{x})} \tag{20}$$

Note that the denominators in Eq.(19) and Eq.(20) are always positive, due to the fact that $0 < H_i(\Phi) < 1$ [16].
- Remaining u_1 and u_2 fixed, and minimising the energy functional $\mathcal{F}(\Phi, u_1, u_2)$ with respect to Φ, we derive the gradient descent flow:

$$\frac{\partial\Phi}{\partial t} = -\lambda\delta\cdot\mathcal{E} - \nu\delta\cdot\mathrm{div}\left(\frac{\nabla\Phi}{|\nabla\Phi|}\right) - \mu\mathrm{div}(d_p(|\nabla\Phi|)\nabla\Phi) \tag{21}$$

where δ is a smooth Dirac function, $\mathcal{E}$ is the function as below

$$\mathcal{E} = (u_1^2 - u_2^2) - c \cdot (u_2 - u_1) \tag{22}$$

where $c = 2 \cdot K_\rho(x) * I(x)$ is a no-negative constant. u_1 and u_2 are given by Eq.(19) and Eq.(20), respectively.

Numerical Implementation and Results

In the section, we will detail the numerical implementation of level-set iterative partial differential equations and parallel GPU implementation by matrix operation. Furthermore, we will discuss the experimental results.

Numerical Implementation

To solve the optimization problem, we employ the simple finite difference scheme to compute $u_1^{(t+1)}(x)$, $u_2^{(t+1)}(x)$ and $\Phi^{(t+1)}$ in an iterative manner:

$$\begin{aligned}
u_1^{(t+1)} &= \left\{ u_1^{(t)} + \frac{K_\rho(x) * [H_1(x) \cdot I(x)]}{K_\rho(x) * H_1(x)} \right\} \Delta t \\
u_2^{(t+1)} &= \left\{ u_2^{(t)} + \frac{K_\rho(x) * [H_2(x) \cdot I(x)]}{K_\rho(x) * H_2(x)} \right\} \Delta t \\
\Phi^{(t+1)} &= \left\{ \Phi^{(t)} - \lambda \delta^{(t)} \left[(u_1^{(t)2} - u_2^{(t)2}) - c \cdot (u_2^{(t)} - u_1^{(t)}) \right] \right. \\
&\quad \left. - \nu \delta^{(t)} \mathrm{div}\left(\frac{\nabla \Phi^{(t)}}{|\nabla \Phi^{(t)}|} \right) - \mu \mathrm{div}(d_p(|\nabla \Phi^{(t)}|) \nabla \Phi^{(t)}) \right\} \Delta t
\end{aligned} \tag{23}$$

where $\mathrm{div}(d_p(|\nabla \Phi|)\nabla \Phi)$ can be found in[21] and Δt is time step.

In practice, the Heaviside function H in Eq. (15) is approximated by a smooth function H_ϵ defined by

$$H_\epsilon(\mathbf{x}) = \begin{cases} \frac{1}{2}\left[1 + \frac{\mathbf{x}}{\epsilon} + \frac{1}{\pi}\sin\left(\frac{\pi \mathbf{x}}{\epsilon}\right)\right], & |\mathbf{x}| \le \epsilon \\ 1, & \mathbf{x} > \epsilon \\ 0, & \mathbf{x} < -\epsilon \end{cases} \tag{24}$$

The derivative of H_ϵ is the following smooth function

$$\delta_\epsilon(\mathbf{x}) = \begin{cases} \frac{1}{2\epsilon}\left[1 + \cos\left(\frac{\pi \mathbf{x}}{\epsilon}\right)\right], & |\mathbf{x}| \le \epsilon \\ 0, & |\mathbf{x}| > \epsilon \end{cases} \tag{25}$$

Parallel GPU Implementation

Taking the iterative level-set convergence into consideration, the computational most expensive operation is the convolution in functions u_1 and u_2 given by Eq. (19) and Eq.(20). Let M is a $l \times m \times n$ matrix, and i, j, k are respectively dimensional subscripts. We could denotes matrix multiplication by element as

$$M(i,j,k) = A(i,j,k) \cdot B(i,j,k) = A_{ijk} \cdot B_{ijk} = M_{ijk} \tag{26}$$

and matrix sum as

$$M^s = \sum_{i=1}^{l} \sum_{j=1}^{m} \sum_{k=1}^{n} M_{ijk} \tag{27}$$

Let $M = \left\{ M_{ijk} \middle| M_{ijk} = K'_{ijk} \cdot f_{ijk}, 1 \le i \le l, 1 \le j \le m, 1 \le k \le n \right\}$, We could decompose M into $a \times b \times c$ blocks of sub-matrices S_{pqr} with dimension $d \times e \times f$ and by definition rewrite convolution as

$$\begin{aligned}
K(\mathbf{x}) * f(\mathbf{x}) &= \sum_{i=1}^{l} \sum_{j=1}^{m} \sum_{k=1}^{n} K'_{ijk} \cdot f_{ijk} \\
&= \sum_{o=1}^{a} \sum_{p=1}^{b} \sum_{q=1}^{c} S^s_{opq} \\
&= M^s
\end{aligned} \tag{28}$$

where, $K'(\mathbf{x}) = K(\mathbf{x} - \mathbf{t})$ and sub-matrix S_{opq} is

$$S_{opq} = \begin{vmatrix} K'_{od+1,\mathrm{pe}+1,\mathrm{qf}} \cdot f_{od+1,\mathrm{pe}+1,\mathrm{qf}} & \cdots & K'_{od+d,pe+1,\mathrm{qf}} \cdot f_{od+d,pe+1,\mathrm{qf}} \\ & \cdots & \\ K'_{od+1,\mathrm{pe+e,qf}} \cdot f_{od+1,\mathrm{pe+e,qf}} & \cdots & K'_{od+d,pe+e,qf} \cdot f_{od+d,pe+pe,qf} \end{vmatrix} \tag{29}$$

In order to compute the convolution operation in using a GPU, we can do the Fast Fourier Transformation(*FFT*) [19] on each GPU *block*(o,p,q) [22] which corresponds to submatrices S_{opq}, and subsequently obtains u_1 and u_2 by sum up all blocks. Therefore, the term $\mathcal{E}$ in Eq.(22), which is a combination of u_1 and u_2, requires no extra computation of convolutions. Note that every matrix operation in our algorithm including matrix sum and element-wise multiplication are simultaneously computed on the GPU by blocks.

Results and Discussion

Data set and settings

We evaluate the proposed method on a 3D images of zebrafish larvae from the Institute of Biology of Leiden University. The set consists 20 of 3D fluorescent images of zebrafish in which every 3D image contains 20 1024×1024 slices, containing a green fluorescent signal. Our implementation environment is: an iMac installed with 64-bit OS X Yosemite, 16 Gigabytes RAM, Intel $Quad - Core^{\mathbf{TM}}$ i7-3770 2.50GHz processor, with one GPU NVIDA GeForce GT 750M. This is a minimal configuration. Our method could be easily extended to a multi-GPU cluster further increasing parallelisation speedup. The experiments were performed in Matlab 2014R and all run-time were recorded in Matlab program.

Evaluation of the Results

We first show the results of our method for zebrafish images in Fig. 2. The initial boundary box and the final boundary surface are shown in the upper row and the lower row, respectively. In the image, the background and the foreground exhibit obvious intensity inhomogeneity and noise. Note that the image is the same as in Fig. 1, in which we have shown that the Piecewise Constant(PC) model and thresholding method are not successful in correctly separating the complete object from the noise. The result in Fig. 2 demonstrates our obvious advantages. In the image, some parts of the fish boundaries are quite weak. As can be seen from (c) and (d) in Fig. 2, our model still achieves satisfactory segmentation result. Fig. 3 shows the maximum intensity projections (MIP) of the fish, which is filled all missing parts on fish body by grey regions, and the rendered volume from our result, which shows the complete extraction from

3D fish data.

In order to provide a detailed demonstration of the advantages of our method on dealing with the low signal-noise ratio phenomenon, we use a single slice from a 3D image. In this 2D slice we show the ability of noise reduction as well as region enhancement. Typically, Fig. 4 shows the result for 2D slice (taken from a 3D image) of quite low signal-to-noise ratio in which a serious intensity inhomogeneity can be observed. For this image, the initial contour was placed across fish body and the background as shown in Fig. 4(a). Here we like to point out that a new contour can emerge and circumscribe even the low-intensity voxels nearby the edge of fish body during the evolution. This can be seen from the curve evolution process as depicted in Fig. 4(b) after 30 iterations. The final contour recovers all boundaries very well, as shown in Fig. 4(c), which is after 50 iterations. From this one can appreciate that our method is also able to segment images consisting of very inhomogeneous regions, which is shown in Fig. 4(d). Note that, the grey part shows that our method could correctly identify unclear voxels located in between the intensity of the signal in the zebrafish and background by using the spatial information and contour length regularity. The application to the zebrafish images comes naturally to our model, it both finds the object while reducing the noise. When the level set function Φ converges, the estimatation fits the original image very well. Moreover, the missing parts on boundaries are filled and, thereby, region partitions are completed.

The result of the level set method provides a segmented

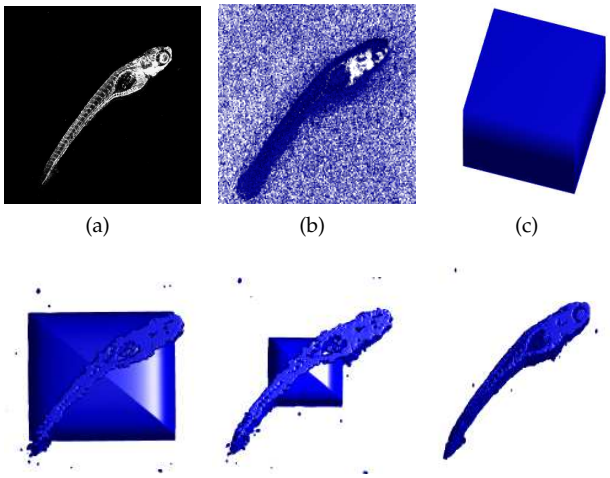

(a) (b) (c) (d) (e) (f)

Figure 2: Application to zebra-fish images. (a): Original data as a 2D projection; (b) 3D object withD noise;(c): Initial boundary box; (d)-(f): surface evolution and Final surface.

region enclosed by contour. As a Consequently, we use the following region-based metric for an evaluation of the segmentation performance [29]. Let R be a segmentation result, and S be the true object region. Denote N_S, N_R, $N_{S\cap R}$ as voxel numbers respectively. We can compute the overlay ratio from the R to the ground-truth region S, denoted by

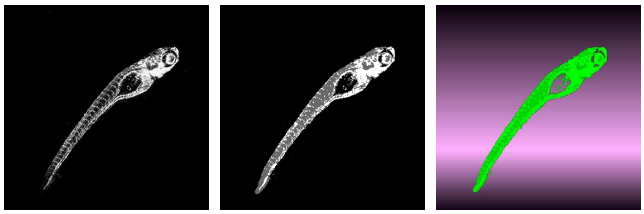

(a) Orignal data (b) Segmentation (c) 3D volume

Figure 3: 3D segmentation result. (a): maximum intensity projection(MIP) of the original data. (b): MIP of the Segmentation. (c): 3D volume after rendering.

$overlay(R,S)$, as follows:

$$overlay(R,S) = \frac{2\cdot N_{R\cap S}}{N_R + N_S} \tag{30}$$

which is referred to as the overlay ratio of R and S. This region-based metric can be used to evaluate accuracy at the voxel-level of a segmentation result. With the above metric, we are able to quantitatively evaluate the performance of our method with different initializations. We applied our method to an image with 20 different initialization contours. In Figure 5, for example, we show three of the 20 initial contours, depicted in white, and their corresponding results, depicted in red. In these three different initializations, initial contour 1 completely includes the object of interest [in Fig. 5(b)], initial contour 2 is in the object [in Fig. 5(c)], and initial contour 3 is completely outside of the object [in Fig. 5(d)]. Despite different locations of these initial contours, the corresponding results are almost the same. All results show the accurate capture of object boundaries. The segmentation accuracy is quantitatively verified by evaluating these results in terms of overlay ratio. The results are shown in Fig. 6(a). This again demonstrates the robustness of our model to the contour initialization.

Complexity Analysis

The images that we use this algorithm for are generally large. Therefore we should consider the extend to which a standard CPU approach would be useful for the processing of large amounts of images. Assume an image contains N voxels. Then, in a sequential implementation, one convolution, according to the definition, for each voxel is $K(x)*f(x)$, costs N^2 times the unit operation. Consequently, each of the N voxels in the image will have its own convolution value of $u_i(x)$ in Eq.(19) and Eq.(20) for every iteration during the convergence procedure. Therefore, the total algorithm complexity in one iteration is $O(N^3)$. If an objective function needs M iterations to obtain convergence, the overall complexity will be $O(M\times N^3)$. Subsequently, even if we use the *FFT* as a substitute for convolution, the computational cost is still up to $O(M\times N^2\log N)$[20]. In order to further accelerate the computation, we could consider this computation as large scale matrix system. Using matrix blocking techniques[27], a convolution operation could be decomposed into K blocks where each block has n voxels as shown in Eq.(28). Our hypothesis is that a GPU could process K blocks in parallel and simultaneously apply *FFT*

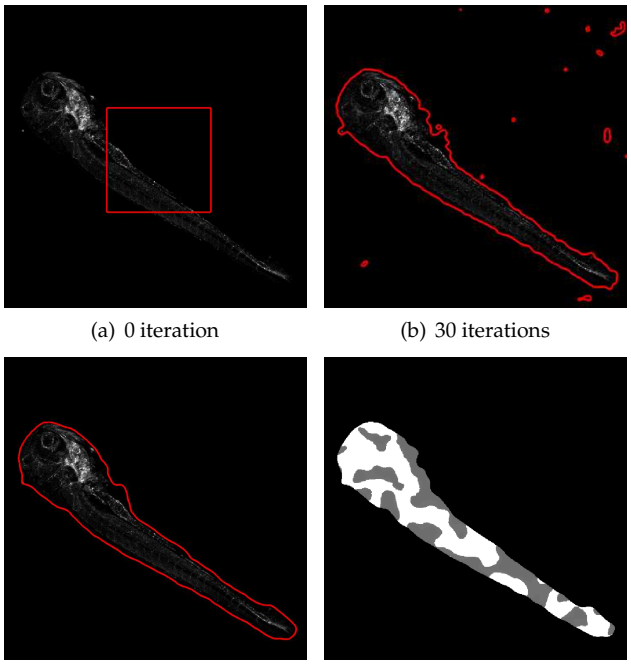

(a) 0 iteration (b) 30 iterations

(c) 50 iterations (d) Estimated result

Figure 4: Application of the level set method to a representative slice from a 3D image of zebra-fish.

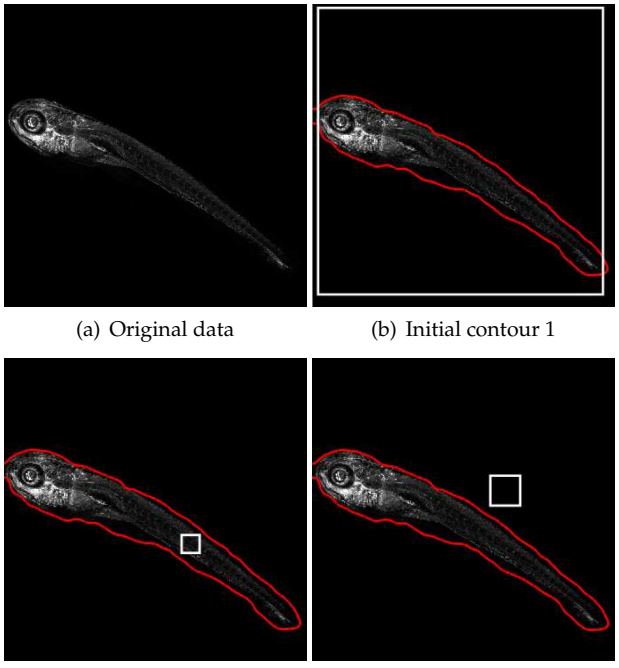

(a) Original data (b) Initial contour 1

(c) Initial contour 2 (d) Initial contour 3

Figure 5: Robustness of our method to contour initializations in a 2D slice. (a)original slice of fish image. (b)-(d)The initial contours, depicted as white contours, and corresponding segmentation results, depicted red contours.

on each blocks. Thus, the complexity of our method as implemented in a parallel manner on GPU has an upper bound $O(M \times \frac{N^2}{(k \cdot n)^2} \log N)$, whereby the computational cost are drastically decreased.

We can quantitatively compare the accuracy of our method using GPU/CPU with that of the PC model by computing the overlay ratio on all 20 3D images. The result of the comparison is shown in the graph of Fig. 6(b). As shown in Fig. 6(b), the overlay ratio of our model is significantly higher than that of the PC model. The CPU implementation of our model is way slower than that of PC model, however, after using parallel GPU acceleration, the run-time drastically decreases; as depicted in Fig.6(c). In our parallellization experiment, our model remarkably speeds up with an average speed-up factor of 11 times; this is listed in Table. 1. Fig.7 shows the good results of our method with one representative image out the all 20 images as an example, and compares it with the PC model. Here it is obvious that our model produces a more accurate segmentation result; 91.68% overlay ratio for our methods against 49.66 overlay ratio for the PC model.

Method	our method		PC
	No GPU	GPU	
Run-Time(s)	9364.57	853.20	453.94
overlay(%)	90.6474	88.9746	49.5923

Table 1: Average run-time,in seconds, and overlay ratio for our method and PC method for all 3D images according to Eq.(30)

Conclusion and Discussion

In this paper, we proposed an algorithm for two-region segmentation. The proposed method is derived from Bayesian inference framework, which efficiently utilizes intensity similarity as well as the spatial location, and combines it with a level-set based approach. This results in a global optimal solution for the two-region case. Therefore, it can segment images with intensity inhomogeneities. The computational complexity can reduced by computing convolution in frequency domain, i.e. *FFT*. In addition, our approach can be further parallelised using GPU's. This results in a drastic reduction of computation time. Our experimental results demonstrate a good performance of our method for images that contain objects with weak boundaries. Comparing our method to a piece-wise constant method clearly illustrates the advantages of our method in terms of efficiency and accuracy.

References

[1] Tomer R, Khairy K, Amat F, Keller P (2012) Quantitative high-speed imaging of entire developing embryos with simultaneous multiview light-sheet microscopy. Nature Methods: 755763.

[2] Mikut R, Dickmeis T, Driever W, Geurts P, Hamprecht F, et al. (2013) Automated processing of zebrafish imaging data - a survey. Zebrafish 10: 401421

[3] Huisken J, Swoger J, Del Bene F, Wittbrodt J, Stelzer EH (2004) Optical sectioning deep inside live embryos by selective plane illumination microscopy. Science 305: 10071009

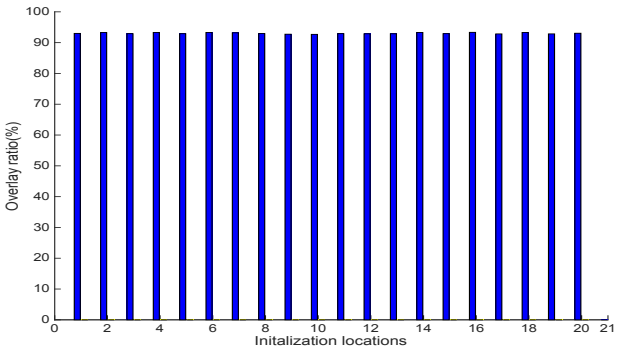

(a) Robustness of initialization locations

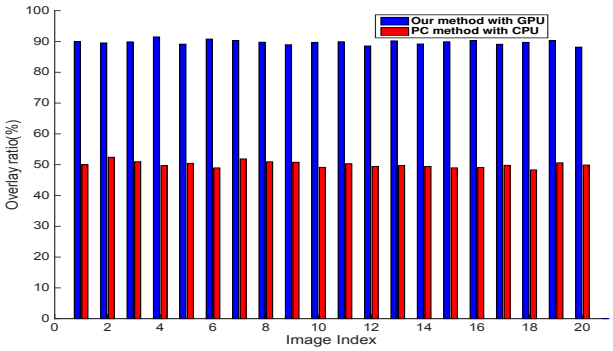

(b) Comparison of overlay ratio

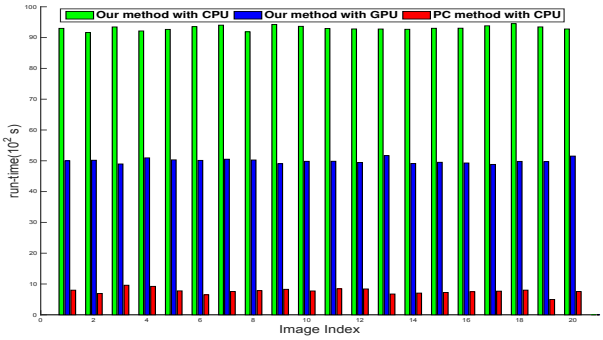

(c) Comparison of computation run-time

Figure 6: (a).Segmentation accuracy of our method for different initialisation locations; (b).Overlay ratio comparison between our method and PC model on all 3D images; (c).Run-time of our method with/without GPU and PC model on all 3D images.

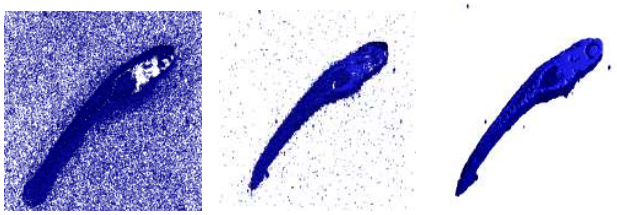

(a) Noised 3D image (b) PC model's result (c) our model's result

Figure 7: Performances of our method compared to PC method. (a): Original 3D image showing noise in the image relevant to the signal; (b): Results of PC method; (c): Results of our method.

[4] Keller P, Schmidt A, Wittbrodt J, Stelzer E (2011) Digital scanned laser light-sheet uorescence microscopy (DSLM) of zebrafish and drosophila embryonic development. Cold Spring Harbor Protocols 2011: pdbprot065839

[5] de Chaumont F, Dallongeville S, Chenouard N, Herv N, Pop S, et al. (2012) Icy: An open bioimage informatics platform for extended reproducible research. Nature Methods 9: 690696

[6] Stegmaier J, Alshut R, Reischl M, Mikut R (2012) Information fusion of image analysis, video object tracking, and data mining of biological images using the open source MATLAB toolbox Gait-CAD. Biomedizinische Technik (Biomedical Engineering) 57 (S1): 458461

[7] Wienert S, Heim D, Kotani M, Lindequist B, Stenzinger A, et al. (2013) CognitionMaster: An object-based image analysis framework. Diagnostic Pathology 8: 34

[8] Zanella C, Campana M, Rizzi B, Melani C, Sanguinetti G, et al. (2010) Cells segmentation from 3D confocal images of early zebrafish embryogenesis. IEEE Transactions on Image Processing 19: 770781

[9] T. Chan and L. Vese, Active contours without edges, IEEE Trans. Image Process., vol. 10, no. 2, pp. 266277, Feb. 2001.

[10] C. Li, C. Kao, J. C. Gore, and Z. Ding, Minimisation of region-scalable fitting energy for image segmentation, IEEE Trans. Image Process., vol. 17, no. 10, pp. 19401949, Oct. 2008.

[11] N. Paragios and R. Deriche, Geodesic active regions and level set methods for supervised texture segmentation, Int. J. Comput. Vis., vol. 46, pp. 223247, 2002

[12] R. Ronfard, Region-based strategies for active contour models, Int. J. Comput. Vis., vol. 13, pp. 229251, 1994.

[13] C. Samson, L. Blanc-Feraud, G. Aubert, and J. Zerubia, A variational model for image classification and restoration, IEEE Trans. Patt. Anal. Mach. Intell., vol. 22, no. 5, pp. 460472, May 2000.

[14] Nieuwenhuis, C., Cremers, D.,Spatially Varying Color Distributions for Interactive Multilabel Segmentation, IEEE Trans. Patt. Anal. Mach. Intell.,Vol. 35 , pp. 1234 - 1247, 2013

[15] Daniel H., Matthias M., Wolfgang S., Differential equation based constrained re-initialization for level set methods, Journal of computational Physics, pp. 6821 - 6845, 2008

[16] Chunming Li, Chenyang Xu, Changfeng Gui, and Martin D. Fox, Level Set Evolution Without Re-initialization: A New Variational Formulation, CVPR, 2005

[17] Paul Tseng, Sangwoon Yun, A coordinate gradient descent method for non-smooth separable minimization, Mathematical Programming, Vol. 117, pp 387-423, 2009

[18] Guely, F., Siarry, P., Gradient descent method for optimizing various fuzzy rule bases, IEEE Int. Conf. on Fuzzy Systems, vol.2, pp. 1241 - 1246, 1993.
[19] Naga K. Govindaraju, Brandon Lloyd, Yuri Dotsenko, Burton Smith, and John Manferdelli, High performance discrete Fourier transforms on graphics processors, Proceedings of ACM/IEEE conference on Supercomputing, Article No.2, 2008
[20] Kenneth Czechowskiy, Casey Battaglinoy, Chris McClanahan, Kartik Iyerz, P.-K. Yeungy; z, Richard Vuducy,On the Communication Complexity of 3D FFTs and its Implications for Exascale, Proceedings of the 26th ACM international conference on Supercomputing, pp. 205 - 214, 2012
[21] Chunming Li, Chenyang Xu, Changfeng Gui, and Martin D. Fox, Distance Regularized Level Set Evolution and its Application to Image Segmentation, TIP, vol. 19 (12), pp. 3243 - 3254, 2010
[22] CUDA NVIDIA Tutorial, NVIDIA CUDA Getting Started Guide for Mac OS X, NVIDIA Corporation, 2015
[23] S.Osher, J.Sethian, Fronts propagating with curvature-dependent speed: algorithms based on Hamilton-Jacobi formulations, J. Comput. Phys, vol. 79, pp. 1249, 1988.
[24] A.Tsai,A.Yezzi,andA.S.Willsky,Curve evolutionimplementation of the MumfordShah functional for image segmentation, denoising, interpolation, and magnification, IEEE Trans. Image Process., vol. 10, no. 8, pp. 11691186, Aug. 2001.
[25] L. Vese and T. Chan, A multiphase level set framework for image segmentation using the Mumford and Shah model, Int. J. Comput. Vis., vol. 50, pp. 271293, 2002.
[26] V. Caselles, R. Kimmel, and G. Sapiro, Geodesic active contours, Int. J. Comput. Vis, vol. 22, pp. 6179, 1997.
[27] Gilbert Strang, Introduction to Linear Algebra, 4th Edition, Wellesley-Cambridge Press and SIAM, 2009
[28] T. Brox and D. Cremers, On the statistical interpretation of the piece- wise smooth MumfordShah functional, in Proc. SSVM, 2007, pp. 203213.
[29] Verbeek, F.J. (1999). Theory & Practice of 3D-reconstructions from serial sections. In Image Processing, A Practical Approach. R.A. Baldock and J. Graham, eds. (Oxford: Oxford University Press), pp. 153-195.

Author Biography

Zhan Xiong received his BS in computer science from the Southwest University, China (2010) and his MS in software application from Southwest University (2013). Now is PhD candidate of Institute of Advanced Computer Science, Leiden University, Netherlands. His work has focused on the biomedical image processing and biomedical data analysis. Fons J. Verbeek did his PhD in the pattern recognition group of the Department of Applied Physics of the Delft University of Technology, The Netherlands. He is Head of the Imaging & BioInformatics group at the Leiden Institute of Advanced Computer Science. His research is in analysis of microscope images and pattern recognition.